Article Subject (see Index Terms below and write one here) _____

Improved Calibration Method of the Photonic Current Sensor for Monitoring HVDC Networks

Alfred Amiolemen[1*], Grzegorz Fusiek.[1**], Pawel Niewczas[1**]

[1] Department of Electronic and Electrical Engineering, University of Strathclyde, Glasgow, United Kingdom
* Student Member, IEEE
** Member, IEEE

Abstract— This letter presents an improved calibration method for a novel optical current sensor (OCS) based on the integration of photonic and piezoelectric technologies to facilitate the distributed measurement of current within High Voltage Direct Current (HVDC) networks. The sensor is designed to fit in an HVDC subsea cable splice to provide remote, distributed current measurement for enhanced monitoring and protection of HVDC power cable assets. The prototype transducer comprises a non-linear amplifier with an enhanced dynamic range to reduce the measurement errors that are dominated by the limitations of the sensor interrogation system at low input signal levels. The improved calibration method incorporates segregated piecewise curve fitting into the sensor calibration characteristic. The experimental results demonstrate significant reduction of the measurement errors showing the potential of the sensor to comply with the accuracy requirements set by the IEC 61869-14 standard for Class 1 DCCT devices.

Index Terms— Low Voltage Transducer (LVT), Optical current sensor (OCS), Direct current transformer (DCCT), High Voltage Direct Current (HVDC), Fiber Bragg Grating (FBG), Piezoelectric Transducer (PZT)

I. INTRODUCTION

The acceleration of the drive towards decarbonization to achieve net zero emissions has spurred innovation across power systems, spanning from generation to utilization. Previously dominated by a vertically integrated structure reliant on carbon-intensive rotating mass for generation, this paradigm is now undergoing deconstruction in favor of distributed generation. This shift introduces a multitude of generation sources, each possessing unique characteristics. However, the proliferation of diverse generation sources presents challenges in aggregating power, necessitating a common transmission corridor or aggregating medium. High Voltage Direct Current (HVDC) emerges as the optimal solution for achieving this objective. Nevertheless, the measurement of network variables in HVDC systems presents challenges, posing threats to network stability and reliability [1], [2], [3]

Also, as compelling as the advantages of HVDC networks are, monitoring the network variables in a distributed fashion for timely detection of developing fault which consequently leads to a fast mitigating action, lacks a mature solution. The sustained fault can be detrimental to HVDC equipment, because of the inherent magnetic energy that can dissipate during fault which can be catastrophic. For example, a typical transport cable with inductance, would generate tons of energy in an HVDC system when 15 kA of fault occurs and is interrupted in a 100 km overhead line. It will theoretically have to cope and absorb up to 11 MJ [4]. [4][5]

For AC networks, fault interruption can be implemented at zero crossing where the magnetic energy is almost at zero, while for DC networks that lack this characteristic, it can be problematic and require even faster reaction times to limit the energy dissipated during

the fault condition [4].

To limit the effect of abnormal fault condition on HVDC network especially in export tie lines, shortening its traveling and rise time will curtail the excessive energy release during fault condition. A shunt embedded within a splice joint which is implemented as an instrument splice joint connector that can measure circuit variables at multiple joints, enhancing improved evaluation of these variables will shorten travel time of fault signal and improve early detection.

Previously, the measurement of these variables in HVDC network has relied on magnetic and shunt-based sensors, each employing distinct principles and operational mechanisms. Magnetic sensors such as fluxgate and Hall effect sensors have been widely adopted in industry, despite encountering challenges such as saturation issues and thermal limitations linked to their Curie temperature. Hybrid sensors combining magnetostrictive elements like Terfenol-D, amorphous ribbon, and fiber Bragg grating (FBG) have also been utilized for DC measurements, yet they suffer from drawbacks including low saturation points and hysteresis. Shunt-based sensors offer solutions to some of these drawbacks, albeit at the expense of galvanic contact [4] - [7].

Integration of shunt-based sensors with the FBG-based Low Voltage Transducer (LVT) within a splice joint forming an instrument splice joint connector, especially within a subsea export tie line, presents an opportunity to enhance the monitoring of these network variables while mitigating the limitations of existing measurement tools [9], [10].

This paper introduces an innovative photonic current sensor (PCS) embedded within a splice connector, serving the dual purpose of joining two conductors and measuring DC network variables. The proposed sensor leverages photonic and piezoelectric technologies for

---

_____

enhanced accuracy and reliability in metrological applications. Characterization of the main circuit complement has been improved by introducing a piece-wise curve fitting into the sensor calibration characteristic. Tests have been conducted in laboratory settings, adhering to the measurement range requirements stipulated by the IEC 61869-14 standard for DC current transformers (DCCT), representing the latest standard for DCCT.

II. HVDC CABLE SPLICE SENSOR

The concept was previously proposed by the authors in [9], [10]. The external view of a bespoke HVDC cable splice enclosure and its internal instrumentation layout with the DC PCS are shown in Fig. 1 without the connection details. The cable terminals are joined by a Manganin shunt. The shunt material is characterized by a low-temperature coefficient of resistivity (10 ppm/K), ensuring high thermal stability of the shunt resistor. The conductor that is being spliced would terminate on either side of the shunt with a resistance of 50 $\mu\Omega$ that would produce a 50-mV voltage drop at the nominal current of 1000 A flowing through the component.
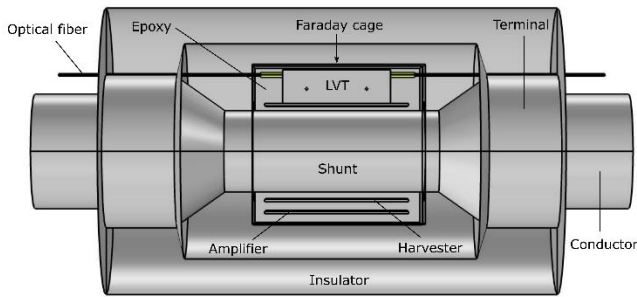

Fig. 1   Conceptual drawing of the instrumented splice joint with its internal components.

The arrangement of the LVT, the energy harvester, and the amplifier in the shunt proximity is shown in Fig. 1 without the connection details. Because the conductor is at high voltage potential while the shunt is surrounded by a sheath at ground potential, the gradient created by this potential difference will expose the components to electromagnetic field which can affect their performance. In order to protect the vulnerable electronics from this field interaction, shielding from the electromagnetic field interference with the form of a Faraday cage as marked in Fig. 1 will be important.

The organized layout and circuit configuration consist of a shunt, harvester, signal conditioner, and LVT, collectively forming a unified solution that functions as an optical current measuring instrument. More details on the sensor concept, explaining the topology, layout, and equations of the components utilized, can be found in [9].

III.   NON-LINEAR AMPLIFICATION

As discussed in [9] , to deliver a nominal voltage of 1 V across the LVT at the nominal current of 1 kA flowing through the shunt, the nominal shunt voltage of 50 mV requires amplification. This was initially realized by means of a linear voltage amplifier based on a non-inverting operational amplifier (op-amp) configuration with a

constant gain of 21 V/V [9]. During the preliminary characterization of the linear op-amp, it was observed that the voltage required at the levels below 20% of the nominal value, were unable to produce sufficient wavelength shifts in the LVT to satisfy the requirements of the measurement accuracy.

A non-linear gain amplifier was proposed, designed and implemented to enhance the lower boundary signal, specifically addressing errors associated with linear signal conditioning in the region below the nominal values. The amplifier characteristics were presented in [9] and the comparison of gain profile between the linear and the non-linear configurations are shown in Fig. 2 plotted in log scale.
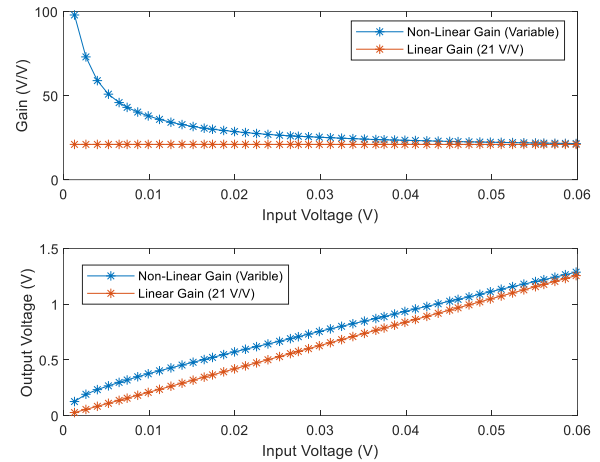

Fig. 2 Input-output characteristic of the amplifiers.

The signals were acquired at 2.5 mV step increment. As can be seen from the comparison between the linear and non-linear amplifiers' input-output characteristics in Fig. 2, the gain of the non-linear amplifier is in the order of 5 times higher than that of the linear amplifier at the beginning of the measurement range and decays with the input (shunt) voltage to reach a gain similar to that of the linear amplifier (21 V/V) at 120% of the nominal voltage (the K_{PCR} value).

Due to the non-linearity of the amplifier, the LVT response to the shunt voltage was also non-linear and the sensor was calibrated using quadratic order polynomials. In [9], it was demonstrated experimentally that the measurement errors at the accuracy limit factor (K_{ALF}) of 3 were achieved with a sufficient margin from specification limits. However, the errors at voltages below the nominal value breached the accuracy limits set by the IEC standard when a standard calibration curve fitting was used. Therefore, an alternative sensor calibration method was proposed ensuring improved measurement accuracy of the sensor, which is reported in the next section.

IV. IMPROVED CALIBRATION AND MEASUREMENT ACCURACY TESTS

Achieving accuracy within the IEC specified boundaries is an important aspect in development of any measurement device. More also that this will be deployed in HVDC network where

_____

monitoring of cable is constituting significant challenge [11], and the challenge exacerbating the difficulty of locating fault point in HVDC cables, which can be expensive in terms of time and resources [12]. It is then critical that the sensor delivers accurate results. This section highlights the steps in achieving this critical component of the process.

A. Experimental procedure

The experimental setup is illustrated in Fig. 3 Fig. 3. A DC source and a resistive voltage divider were used to emulate shunt voltage in an HVDC line. The requisite voltage across the shunt resistor constituted an input for both the harvester and the amplifier. The LVT sensor was connected to the output of the amplifier and optically interrogated by an IBSEN superluminescent light-emitting diode (SLED) source and spectrum analyzer (I-MON USB 256).
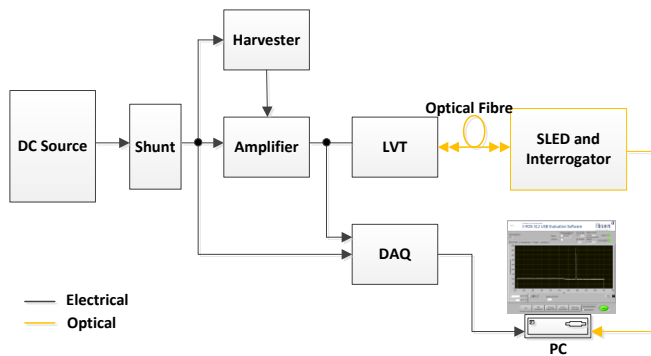

Fig. 3 Experimental setup

A data acquisition (DAQ) card (NI 6003) was utilized to acquire electrical signals from the amplifier and the shunt for calibration purposes. The acquisition speed for the electrical signals was set to 3 ksps to match the LVT interrogation at 3 kHz, and the signals were logged for subsequent signal processing and analysis.

B. Sensor calibration curve

To calibrate the sensor, the shunt voltage together with the LVT wavelength response were arranged as shown in Fig. 4 plotted in log scale. Clearly, the non-linear gain amplifier characteristic causes a non-linear relationship between input (shunt voltage) and output (LVT wavelength) signals of the sensor as mentioned earlier.

Initially, a direct polynomial fitting ranging from 2nd to 6th order was attempted and fitted into the averaged LVT hysteresis loops (see Fig. 4 (a)), but the results failed to meet the error limits required by the IEC standard. Therefore, it was proposed to employ a method of segregated piecewise polynomial fitting, one for the non-linear section and another for the linear section up to a measurement range of 300% of the nominal voltage which also represent the K_{ALF} value.

The measurements were taken across two ranges 0-120% and 120%-300% of the nominal voltage. The data was then merged in the post-processing to obtain the curve shown in Fig. 4 (a).

Consequently, the calibration curve was created by segregated piecewise polynomial fitting with a confidence level of 95%. Each measurement point was achieved as an average of 3000 samples.

The segregated piecewise polynomial fittings are shown in Fig. 4

(b). The more non-linear part of the sensor calibration curve at lower voltages (0-20%) was fitted with a 2nd order polynomial with different coefficients (marked in red in Fig. 4 (b)) than the remaining range of the calibration curve where the response was more linear. This also required 2nd order polynomial fitting (marked in green in Fig. 4 (b)) but with smaller values of the polynomial coefficients.
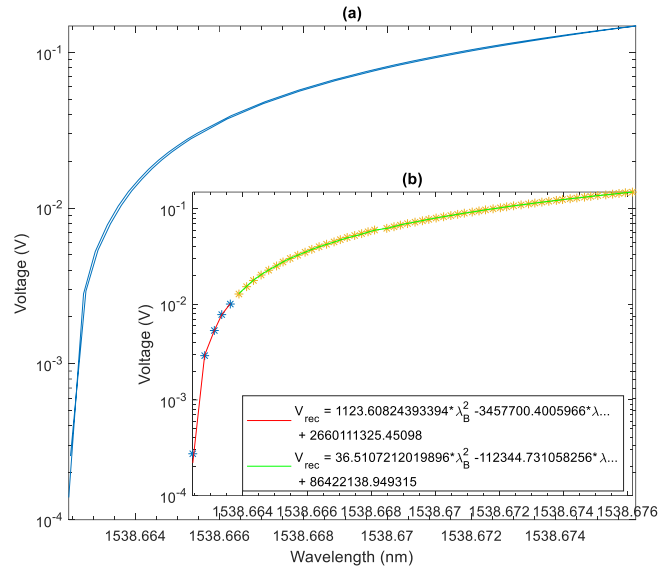

Fig. 4 Sensor calibration curve and hysteresis loop

Consequently, the resultant calibration curves' equations were implemented in the signal processing software to verify the sensor measurement accuracy for signals up to 300% of the nominal conditions.

C. Ratio (amplitude) errors

The sensor measurement accuracy was assessed based on the estimation of the ratio (amplitude) error, ε_r, using the following equation:

$$\varepsilon_r(\%) = \frac{V_{ref} - V_{rec}}{V_{ref}} \times 100 \tag{3}$$

where V_{ref} and V_{rec} are reference (shunt) and reconstructed voltage, respectively.

In accordance with the requirements of the IEC 61869-14 standard, the errors were estimated at 5%, 20%, 100%, 120% (K_{PCR}) and 300% (K_{ALF}) of the nominal conditions. The accuracy up to a k_{ALF} of 3 was within the required limits, as demonstrated in Fig. 5, Simple Acceptance Rule with the Guard Bands equal to zero was used to test the error conformity to basic error analysis. Consequently, if the error (or mean error) is within the specified limits, as we showed in our plot, it means that the statement of conformity is "pass".

As stated in previous section, the calibration curve was created by segregated piecewise polynomial fitting with a confidence level of 95%. The way the errors are presented shows the repeatability of the measurement for three

_____

consecutive runs.

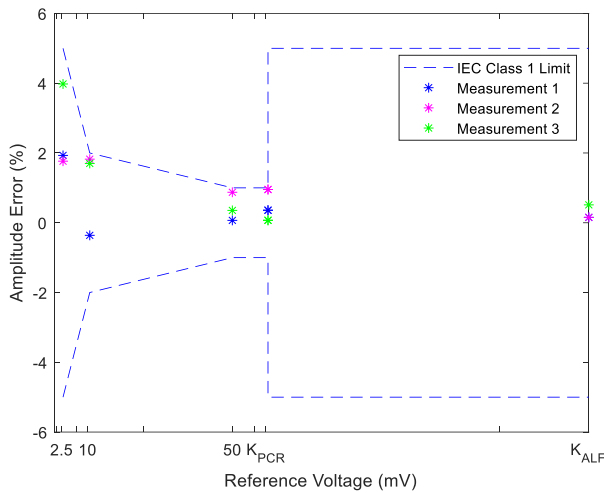Clearly, the measurement error is lower for a higher signal-to-noise (SNR) ratio.

Fig. 5 Sensor amplitude errors up to 300% of the nominal compared to the error limits set by IEC 61869-14 for Class 1 devices.

As can be seen from the presented results, the amplitude errors for the voltages up to 300% of the sensor nominal value have been improved in comparison to those presented by the authors in [9] and are within the error limits set by IEC 61869-14 for Class 1 DCCT devices [10], [13]

V. CONCLUSION

This paper has shown the details of improved calibration method used for achieving an accuracy that meet IEC standard for DCCT on this proposed instrument splice joint connector. Upon full development of this sensor designed for integration into splice joints, it will enhance the measurement of network variables, thereby improving network visibility and facilitating wide-area network monitoring. This advancement will be a key enabler to cable condition monitoring, allowing for the detection of patterns and irregular parameter signatures. Additionally, it will help to mitigate the propagation duration of fault currents, which can have catastrophic consequences on DC equipment if sustained for more than 10 ms [4]. The circuit's response to fault/transient currents has been previously documented [9].

While the final comprehensive solution remains an ongoing effort, with a focus on thermal and electrical modeling of the instrument splice, the characterization of internal components and laboratory testing have yielded results consistent with IEC standards. The sensor is a self-sustaining solution, powered by energy scavenged from the shunt. Moreover, the sensor has the potential of being multiplexed together with similar sensors, forming a distributed current measurement capability.

VI. ACKNOWLEDGEMENT

REFERENCES

[1] M. Barnes, D. van Hertem, S. P. Teeuwsen, and M. Callavik, "HVDC Systems in Smart Grids," 2017.

[2] ABB, "ABB review, HVDC special report," 2014.

[3] SP Networks, "ANGLE-DC 2015 Electricity Network Innovation Competition," 2015.

[4] R. P. P. Smeets and N. A. Belda, "High-voltage direct current fault current interruption: A technology review," Apr. 01, 2021, *John Wiley and Sons Inc*. doi: 10.1049/hve2.12063.

[5] M. A. Paun, J. M. Sallese, and M. Kayal, "Hall effect sensors design, integration and behavior analysis," *Journal of Sensor and Actuator Networks*, vol. 2, no. 1, pp. 85–97, Mar. 2013, doi: 10.3390/jsan2010085.

[6] TI, "Introduction to Hall-Effect Sensors," 2023. [Online]. Available: www.ti.com

[7] K. Maniar, "Comparing Shunt-and Hall-Based Isolated Current-Sensing Solutions in HEV/EV," 2023. [Online]. Available: www.ti.com

[8] P. Weßkamp and J. Melbert, "3.4.4 - High Performance Current Measurement with Low-Cost Shunts by means of Dynamic Error Correction," AMA Service GmbH, Dec. 2020, pp. 224–230. doi: 10.5162/sensoren2016/3.4.4.

[9] A. Amiolemen, G. Fusiek, and P. Niewczas, "Towards the Development of a Photonic Current Sensor for HVDC Networks."

[10] A. Amiolemen, G. Fusiek, and P. Niewczas, "Self-Powered Signal Conditioning Circuit for an HVDC Optical Current Sensor," *IEEE Sens Lett*, pp. 1–4, Sep. 2023, doi: 10.1109/lsens.2023.3311676.

[11] Dr Othmane El Mountassir, "HVDC transmission cables in the offshore wind industry: reliability and condition monitoring," 2015. [Online]. Available: http://www.tennet.eu/nl/news/article/tennet-and-mitsubishi-corporation-extend-partnership-in-ger-

[12] ENTSO-E, "ENTSO-E AISBL Recommendations to improve HVDC cable systems reliability Recommendations to improve HVDC cable systems reliability," 2019.

[13] IEC 61869-14, "INSTRUMENT TRANSFORMERS-Part 14: Additional requirements for current transformers for DC applications (SASO)," 2019.